JOURNAL OF SPACECRAFT AND ROCKETS
Vol. 44, No. 5, September–October 2007

Approximate Trajectories for Thermal Protection System Flight Tests Mission Design

Urbano Tancredi* and Michele Grassi†
University of Naples "Federico II," 80125 Napoli, Italy

DOI: 10.2514/1.22007

A mission profile for advanced thermal protection system suborbital flight testing is identified. Its main goal is to achieve a constant heat flux at a specific area of the vehicle for a limited amount of time. A tool capable of exploring broad regions of the design space for these missions is developed, aiming at reducing possible design options to an extent manageable by conventional, more accurate, numeric-simulation-based methods. Based on a simplified model of the point mass dynamics, trajectories optimal for thermal protection system testing and compliant with prefixed path constraints are identified. The approximate method is validated comparing the obtained optimal trajectories with numeric-optimized standard solutions on three test cases. Then, to demonstrate the method effectiveness and flexibility, the mission design space is investigated for reasonable ranges of relevant parameters. Results show that increasing the vehicle's ballistic coefficient allows reducing the specific mechanical energy at reentry, and that the maximum admissible dynamic pressure plays a principal role in affecting the attainable testing performances. An illustrative mission design for novel ceramic thermal protection system testing is presented that minimizes in the analyzed design space the specific mechanical energy at the trajectory apogee.

Nomenclature

B	=	ballistic coefficient
C	=	heat flux constant
E	=	specific mechanical energy
f	=	generic function
g	=	gravitational acceleration
h	=	altitude
k	=	proportionality constant
L/D	=	vertical lift-to-drag ratio
L_T/D	=	aerodynamic efficiency
$\dot{q}$	=	stagnation point heat flux
$\bar{q}$	=	dynamic pressure
$\bar{q}_{\text{Atm}}$	=	minimum dynamic pressure for atmospheric flight
$\bar{q}_{\max}$	=	maximum admissible dynamic pressure
$\dot{q}_{\text{TPS}}$	=	stagnation point heat flux desired for TPS test
R	=	Earth's equatorial radius
R_N	=	stagnation point curvature radius
r	=	radial distance from Earth's center
t	=	time
u	=	input vector
V	=	velocity
x	=	state vector
β	=	exponential atmosphere scale factor
γ	=	flight path angle
Δ	=	Loh's constant
Δt	=	TPS test time
μ	=	Earth's gravitational parameter
ρ	=	atmospheric density
$\tilde{\rho}$	=	atmospheric density at which the test heat flux is reached flying at the maximum admissible dynamic pressure
ρ_q	=	atmospheric density at which dynamic pressure constraint avoidance maneuver starts
ρ_{sl}	=	sea-level atmospheric density
ρ_T	=	maximum atmospheric density at which desired heat flux can be tracked

Subscripts

$()_A$	=	trajectory apogee value
$()_{\text{Kep}}$	=	Keplerian phase value
$()_{\text{PU}}$	=	pull-up maneuver value
$()_{\text{TPS}}$	=	TPS test value
$()_0$	=	atmospheric entry interface value
$()_1$	=	heat flux trim acquisition value
$()_2$	=	TPS test end value

I. Introduction

THE thermal protection system (TPS) is one of the most critical subsystems in vehicles performing an atmospheric reentry. Hence, a high confidence level must be acquired before integration of this subsystem into a flight vehicle. This requires intensive ground and flight testing activities to validate novel TPS concepts. TPS ground testing poses several nontrivial challenges, mainly related to the reproduction of the aerothermal flight conditions. Purposely conceived ground facilities are required to replicate the challenging aerothermal environment. Usually the resulting plants [1] are huge, complex, and remarkably costly to develop and operate. In light of these difficulties, the capability to reproduce on ground the reentry flight aerothermal environment is still significantly limited [2]. As a consequence, the flight demonstration of a ground validated TPS has some degree of associated risk. Specifically designed flight tests are thus a viable alternative.

To acquire thorough confidence in the TPS performance, the most effective flight test strategy is to perform a reentry from an orbital (or near-orbital) initial state, flying in aerothermal conditions close to the ones in which the TPS is intended to operate. On the other hand, such a testing approach requires one to perform an entire atmospheric reentry, with resulting high cost and complexity. Nonetheless, these must be kept low when dealing with a subsystem flight test, or a high risk technology demonstration, as in the case of novel TPS validation. Indeed, recent examples of this strategy either incorporate testing of several reentry subsystems, as in the case of the Japanese orbital reentry experiment (OREX) flight [3], or are designed for thorough characterization of the reentry aerothermal environment by

Received 23 December 2005; revision received 25 February 2007; accepted for publication 3 June 2007.

*Contract Researcher, Department of Aerospace Engineering, Piazzale Vincenzo Tecchio 80. Member AIAA.

†Associate Professor, Department of Aerospace Engineering, Piazzale Vincenzo Tecchio 80.

means of multiple experiments, as for the upcoming European experimental reentry test bed (EXPERT) mission [4].

Thus, atmospheric reentry from orbital or high-energy suborbital conditions does not seem a viable option for flight testing of advanced TPS by means of a purposely designed mission. Hence, we do not cover these cases in the present paper. Significant savings in the resources needed to perform a TPS flight test can be obtained if the flight reaches only low-energy suborbital conditions, possibly making maximum use of off-the-shelf vectors, such as ballistic missiles or sounding rockets [5,6]. The main drawback of this flight testing strategy is that TPS testing is carried out in a similar, but different, aerothermal environment. For instance, the heat flux time profile differs from reentry ones, even if the values can be comparable. The trajectory covers different Reynolds number and dynamic pressure regions, which influence the onset of complex phenomena, such as boundary-layer transition. It is clear that this difference between the flight test conditions and the operating ones shall be taken into account for test results' interpretation. This is thought to be an important issue in such a testing strategy. Nonetheless, this subject is beyond the scope of the present paper that is intended to focus on simplified models for mission analysis and design of such flight tests. Recent examples of suborbital TPS flight tests include the German sharp edge flight experiment (SHEFEX) mission [6], whose main focus is on hypersonic aerothermodynamic data gathering for faceted surfaces and sharp edges, NASA's slender hypersonic aerothermodynamic research program (SHARP-B) [7], and the suborbital reentry test (SRT) of the unmanned space vehicle program [8], currently under development at the Italian Aerospace Research Center (CIRA).

All of these missions experience an extremely variable heat flux time profile, typical of low aerodynamic efficiency orbital reentry flights, although heat flux values are lower due to the sensibly smaller specific mechanical energy. Conversely, in a lifting reentry the heat flux tends to be more constant during the maximum heat flux flight portion [9]. In the present work we will focus on a testing approach that is somehow in between a complete atmospheric reentry and the suborbital ballistic flights just mentioned. Specifically, the flight test starts as well from low suborbital energy levels, but is designed to obtain constant heat flux conditions on a TPS sample. This approach allows a better characterization of the TPS behavior versus input heat fluxes in conditions more similar to lifting reentry, and simplifies the test results interpretation that benefits from the constant thermal input.

Suborbital TPS flight tests constitute a peculiar application from the point of view of trajectory determination. To replicate the heat flux values typical of atmospheric reentry, the trajectory shall be designed to maximize the aerothermal stress on the vehicle, exactly the opposite of what is customarily done in reentry trajectory design. More precisely, atmospheric reentry trajectories are usually determined constraining, among others, the heat flux of some vehicle's specific point(s) to be lower than a given threshold, dictated by the selected TPS materials. Then, the trajectory is obtained minimizing the integrated heat load on the vehicle, which mainly determines the TPS mass. For suborbital flight tests, given the lower energy levels, the integrated heat load is not the primary concern. To obtain the lowest launch energy that realizes the desired aerothermal environment, the aerothermal stress experienced by the vehicle shall thus be maximized.

Given the peculiarity of these applications, there is the need of developing appropriate mission analysis tools, for example, capable of determining, for desired TPS testing flight conditions, the specific mechanical energy levels and the vehicle's aerodynamic characteristics needed to satisfactorily perform the flight test. Previous studies related to similar missions have been focused on the specific system and mission needs, by applying and/or adapting conventional mission and trajectory design techniques typical of reentry problems [10,11]. A parametric analysis is performed in the mission design space, making use of local numeric optimization schemes for trajectory design, carried out via massive numeric dynamics simulations [10–13]. The main limitation of these techniques is the capability of exploring only a limited number of candidate solutions in the mission design space that are usually identified based on the legacy of similar missions. In applications that do not benefit from previous experiences, such as those we refer to, the design space to be evaluated by parametric analysis is often restricted by means of heuristic interpretation of the underlying physics. In this context, a tool capable of exploring broad regions of the mission design space would be extremely helpful in narrowing the possible design candidates to an extent manageable by numeric-simulation-based methods. To the authors' knowledge, no such tools have ever been developed to aid in investigating optimal mission designs for constant heat flux suborbital TPS flight tests.

The objective of the present paper is to derive a method capable of performing mission analysis over a wide portion of the design space of such missions, by means of simplified analytical dynamics models suitable to identify optimal trajectories. The tool is intended for a mission design phase, being more flexible than numeric-simulation-based methods in analyzing broad regions of the parameter's design space. The purpose of the method is to assess the main features of a mission design capable of meeting the desired performances, to determine design candidates for further analysis. Therefore, it should be considered as preparatory and complementary to more accurate numeric-simulation-based methods. In the following, a class of trajectories is identified that responds to the TPS testing requirements, on which dynamics modeling issues are analyzed. A simplified, semi-analytic model of the point mass dynamics in the longitudinal flight plane is proposed. Based on this model, trajectories optimal for TPS testing and compliant with given path constraints are identified. Then, the accuracy of the simplified approach is evaluated by comparison with numeric-optimized standard solutions on three test cases. Finally, to exemplify the method effectiveness and flexibility, the mission design space is investigated for reasonable ranges of relevant parameters, yielding to trajectory initial conditions that allow performing the TPS flight test as desired.

II. Simplified Dynamics Models

As usually done in mission design phases, a point mass dynamics model is used to describe the vehicle's trajectory. In addition, only the motion in the longitudinal plane is considered, because no requirements are imposed on the trajectory cross range. The resulting dynamics is described by a 2 degrees of freedom (DOF) model, whose representation can be given as in Eq. (1). We emphasize that L/D stands for the ratio between the lift vertical component and drag, whereas the vehicle's aerodynamic efficiency is denoted by L_T/D,

$$\dot{x} = f(x, u) \qquad x = (V, \gamma, \rho)^T \qquad u = (L/D, B)^T \qquad (1)$$

The point mass motion is described as a planar entry flight over a spherical, nonrotating planet with constant gravity acceleration, exponential atmospheric density, and zero thrust [14]. Concerning aerothermal modeling issues in atmospheric entry mission analysis and trajectory design, heat flux requirements are usually expressed in terms of the heat flux at one (or more) stagnation point [15–17]. Of course, because the TPS sample to be tested extends beyond the stagnation point, the incoming heat flux distribution over the testing area shall be determined as well. Computation of this distribution shall take into account complex mutual dependencies among vehicle geometry, surface characteristics, and flight conditions [18]. Heavy nonlinear phenomena can also occur, such as boundary-layer transition, whose accurate prediction is still an active research topic [19]. Taking into account the incoming heat flux distribution thus requires a detailed knowledge of the system features. This prevents dealing with this subject in a mission design context. On the other hand, formulating TPS test requirements in terms of the stagnation point heat flux assures that the desired thermal input is obtained at the stagnation point. In addition, only system-level information is required to compute its value. Hence, we enforce TPS requirements referring only to the stagnation point heat flux, determined by means of the well-known Fay–Riddel formulation [20]:

$$\dot{q} = C\sqrt{\rho/R_N}\cdot V^3 \tag{2}$$

The u vector in Eq. (1) characterizes maneuvering capability of the vehicle. We assume that the aerodynamic shape of the vehicle is given, whereas its surface to mass ratio is a design parameter we wish to determine. Moreover, we suppose the trajectory is flown at a constant angle of attack. The angle of attack substantially affects the aerothermal field surrounding the vehicle and the incoming heat flux distribution on its surface. For advanced TPS testing is highly desirable to have the test heat flux confined to a specific area of the vehicle, where the TPS sample is placed. This constrains the angle of attack to be somewhat near a certain value, ruling out angle of attack guidance. As a consequence, the ballistic coefficient can be assumed to be constant along the trajectory. Its value is determined by the vehicle's mass to surface ratio and the drag coefficient arising from the selected angle of attack. We thus assume that the vehicle maneuvers by rolling the lift vector about the velocity vector, a control technique known as bank modulation. In this way the vehicle can fly anywhere between a full lift up (0 deg bank) and full lift down (180 deg bank) orientation as required for trajectory tracking. As a consequence, the L/D on a generic point of the trajectory is between the negative and positive L_T/D corresponding to the chosen angle of attack. It is worth noting that, to benefit from higher maneuvering capability, the angle of attack should be selected to maximize the aerodynamic efficiency.

Because the trajectory is conceived to maximize the aerothermal stress on the vehicle, the ascent phase ends outside the atmosphere, to minimize launch energy losses. A wealth of analytic methods is available for ascent dynamics description [14]. We thus restrict the analysis to the reentry phase of the flight. In other words, we assume that the mission starts at the trajectory "apogee," where the altitude is maximum and the flight path angle is zero.

To obtain the equations of motion in closed form, the mission profile is split into three main phases. This is achieved by dividing the trajectory into three segments: a Keplerian phase, lasting until aerodynamics forces become significant; a pull-up maneuver, executed to achieve constant-$\dot{q}$ conditions for TPS testing; and a TPS test phase, performed at constant heat flux. As a result, we obtain three different simplified dynamics models that patched together yield the complete equations of motion. An interpretation is given in Fig. 1, where a typical trajectory is shown in the density, velocity plane.

For the sake of clarity, in the following sections the three models are introduced starting from the last trajectory segment.

A. TPS Test Phase

We assume that the TPS test is carried out on a trajectory with small flight path angles. As will be clearer later on, this is because aerothermal stress maximization requires a trajectory as horizontal as possible. The gravity tangential component can thus be neglected. The resulting equations of motion can be written in local form as

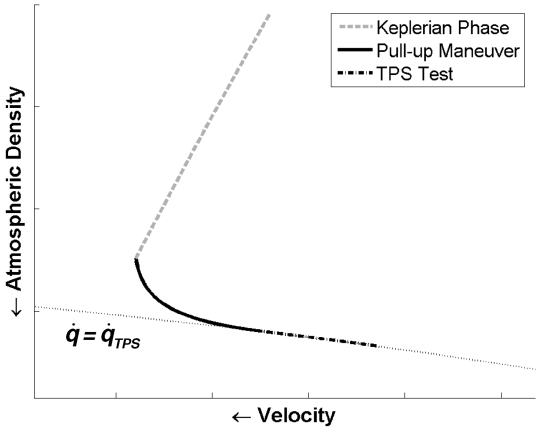

Fig. 1 Typical TPS flight test reentry trajectory.

$$\mathrm{d}V/\mathrm{d}\rho = V/2\beta\gamma B \tag{3}$$

$$d(\cos\gamma)/\mathrm{d}\rho = \frac{L/D}{2\beta B} - \frac{(gR/V^2 - 1)}{\rho\beta R} \tag{4}$$

Enforcing heat flux trim conditions by means of Eq. (2), the velocity and flight path angle become a function of the atmospheric density:

$$V_{\mathrm{TPS}}(\rho) = k\rho^{-1/6}; \qquad \gamma_{\mathrm{TPS}}(\rho) = -3\rho/\beta B \tag{5}$$

$$k := (\dot{q}_{\mathrm{TPS}}\sqrt{R_N}/C)^{1/3} \tag{6}$$

From Eqs. (3) and (6), we can arrive at an expression for the time spent flying between two points on a constant heat flux trajectory. Using the kinematic relationship between altitude and flight path angle, after some manipulations we get

$$\Delta t = 2B\left(\rho_1^{-5/6} - \rho_2^{-5/6}\right)/5k \tag{7}$$

Thus, aerothermal stress maximization can be viewed either as maximizing the test heat flux, that is, maximizing k for a given test time Δt, or, conversely, maximizing Δt for a given k. Equation (7) implies that both these two alternative formulations require B maximization. This, in turn, requires a constant-$\dot{q}$ trajectory as horizontal as possible [see Eq. (5)].

To track the constant-$\dot{q}$ trajectory, the vehicle shall have the necessary maneuvering capability. Tracking a constant-$\dot{q}$ trajectory requires a specific L/D at each atmospheric density, depending on the ballistic coefficient value. Indeed, substituting the trajectory Eq. (5) in Eq. (4) and rearranging in terms of the vertical lift-to-drag ratio yields

$$L/D_{\mathrm{TPS}} = \frac{2B}{R\rho}\cdot\left(\frac{gR}{k^2}\rho^{1/3} - 1\right) - \frac{18\rho}{\beta B} \tag{8}$$

As a matter of fact, to track the constant heat flux trajectory, the requested L/D_{TPS} shall be within $\pm L_T/D$. To estimate the density range in which this condition is met, we assume L/D_{TPS} is a monotone decreasing function of the atmospheric density. Inspection of Eq. (8) shows that this holds as far as the centripetal acceleration due to Earth's curvature having a secondary effect. Although this is true for low-energy suborbital flight, this assumption shall be carefully applied when dealing with near-orbital specific mechanical energy levels. In fact, in closed orbits this term balances the gravitational acceleration effect. As a consequence of this simplification, the minimum and maximum densities between which the vehicle can track $\dot{q}_{\mathrm{TPS}}$ are obtained by substituting in Eq. (8) positive and negative L_T/D, respectively. For instance, the maximum trackable density ρ_T satisfies the following nonlinear scalar equations that can be solved by means of a numeric root finding scheme:

$$\frac{2B}{R\rho_T}\cdot\left(\frac{gR}{k^2}\rho_T^{1/3} - 1\right) - \frac{18\rho_T}{\beta B} + L_T/D = 0 \tag{9}$$

B. Pull-Up Maneuver

The model used to describe this trajectory segment is known as Loh's model [21], originally conceived for atmospheric reentry. It can be derived by the 2-DOF point mass model by assuming that the gravity tangential component is negligible and the difference between centripetal and vertical accelerations due to gravity is constant along the maneuver.

$$\Delta := 2(gR/V^2 - 1)\cos\gamma/\rho R \cong \mathrm{const} \tag{10}$$

Loh's model additionally assumes constant aerodynamic inputs, thus arriving at the closed form Eqs. (11) and (12). Thus, we refer to a pull-up maneuver performed with constant L/D, that is, with a constant bank angle.

$$V_{\mathrm{PU}}(\rho) = V_0 \cdot \exp\left(\frac{\gamma_0 - \gamma_{\mathrm{PU}}(\rho)}{L/D_{\mathrm{PU}} - \Delta \cdot B}\right) \tag{11}$$

$$\gamma_{\mathrm{PU}}(\rho) = \cos^{-1}\left[\cos\gamma_0 + \frac{1}{2\beta}\left(\frac{L/D_{\mathrm{PU}}}{B} - \Delta\right) \cdot (\rho - \rho_0)\right] \tag{12}$$

Because the pull-up maneuver is executed to acquire heat flux trim conditions, it ends on the constant heat flux trajectory segment. Enforcing this patching condition in Eqs. (11) and (12) and rearranging, we obtain the analytic expressions relating the pull-up initial conditions to the trim acquisition state by means of the applied trajectory inputs:

$$L/D_{\mathrm{PU}} = \Delta \cdot B + (\gamma_0 + 3\rho_1/\beta B)/\ \ell_n\left(k\rho_1^{-1/6}/V_0\right) \tag{13}$$

$$2B\beta - \frac{\gamma_0 + 3\rho_1/\beta B}{\cos(-3\rho_1/\beta B) - \cos\gamma_0} \cdot \frac{\rho_1 - \rho_0}{\ell_n(k\rho_1^{-1/6}/V_0)} = 0 \tag{14}$$

C. Keplerian Phase

In this phase the point mass dynamics are assumed to be adequately described by the Keplerian model. Unlike the two preceding models, it uses the inverse-square gravity approximation. For our purposes, it is convenient to define the zero reference of gravity potential energy at zero altitude. Hence, given the apogee radius and the specific mechanical energy, we obtain the velocity and flight path angle as a function of either altitude, or atmospheric density via the exponential model:

$$V_{\mathrm{Kep}}(\rho) = \sqrt{2[E - \mu(R^{-1} - r(\rho)^{-1})]} \tag{15}$$

$$\gamma_{\mathrm{Kep}}(\rho) = \cos^{-1}\left(\frac{r_A}{r(\rho)} \cdot \sqrt{[E - \mu\left(R^{-1} - r_A^{-1}\right)]/[E - \mu(R^{-1} - r(\rho)^{-1})]}\right) \tag{16}$$

$$r(\rho) = R - \beta^{-1}\ \ell_n(\rho_{\mathrm{sl}}/\rho) \tag{17}$$

The Keplerian phase ends when the drag loads due to the aerodynamic pressure become significant with respect to gravity [22]. This condition is here expressed in terms of dynamic pressure, that is, when the dynamic pressure exceeds a threshold value the Keplerian model ceases to be valid. In this way, the density at which the flight becomes atmospheric can be obtained by specifying an appropriate dynamic pressure threshold. This yields to the nonlinear Eq. (18), whose solution ρ_0, computed by a numeric root finding scheme, allows one to determine the patching conditions with the pull-up maneuver via Eqs. (15) and (16):

$$\rho_0\left[E - \mu\left(\frac{1}{R} - \frac{\beta}{\beta R - \ell_n(\rho_{\mathrm{sl}}/\rho_0)}\right)\right] - \bar{q}_{\mathrm{Atm}} = 0 \tag{18}$$

III. Approximate Model Formulation and Trajectory Determination

To correctly estimate the performance achievable by a generic mission design, the trajectories on which the approximate method is based are determined solving an optimization problem, in which the merit function is the aerothermal stress on the test material. As pointed out in Sec. II.A, this is equivalent to maximize the TPS test time.

Path constraints are enforced on the maximum heat flux and the maximum dynamic pressure. Because we refer to advanced TPS testing applications, the desired test heat flux is also the maximum the TPS can sustain without damage. The heat flux constraint is thus implicitly satisfied requiring one to fly in the proximity of its test value. Furthermore, it can be shown that the maximum dynamic pressure constraint specifies a maximum density above which the TPS test cannot take place.

A constant dynamic pressure specifies a curve in the V–ρ plane. To comply with the constraint, the vehicle shall fly geometrically above that curve, that is, at densities lower than the one on the maximum dynamic pressure curve for each velocity value. The constant heat flux specifies a curve in the V–ρ plane as well, and there is a unique point in which the two curves intersect:

$$\tilde{\rho} = (\sqrt{2\bar{q}_{\max}}/k)^3 \tag{19}$$

For densities lower than $\tilde{\rho}$, the constant-$\dot{q}$ curve is geometrically above the constant-$\bar{q}$ one. Therefore, to comply with the maximum dynamic pressure constraint, the TPS test can be performed only at densities lower than $\tilde{\rho}$. Nevertheless, this condition does not guarantee by itself compliance with the dynamic pressure constraint. Indeed, a flight path angle discontinuity occurs at the intersection point between the $\dot{q}_{\mathrm{TPS}}$ and the $\bar{q}_{\max}$ curves that has to be taken into account. Proceeding as in Sec. II.A, we can express the flight path angle required to fly on the $\bar{q}_{\max}$ curve as

$$\gamma|_{\bar{q}=\mathrm{const}} = -\rho/\beta B \tag{20}$$

Comparing Eqs. (5) and (20) it is seen that a constant heat flux curve requires a steeper flight path than a constant dynamic pressure one. To transfer from the $\dot{q}_{\mathrm{TPS}}$ to the $\bar{q}_{\max}$ curve the vehicle shall execute an additional pull-up maneuver. This maneuver shall start at a density adequately lower than $\tilde{\rho}$, so that it is possible to increase the flight path angle at least up to the $\bar{q}_{\max}$ curve. The maximum dynamic pressure constraint effect is thus to specify a superior limit to the density range in which the TPS test can take place.

An estimate of the test end density is obtained introducing additional simplifying assumptions. Specifically, we refer to an "efficient" pull up, that is, that allows performing the TPS test up to the highest possible density. This implies the maneuver makes use of maximum vertical lift-to-drag ratio, and the resulting trajectory is tangent to the $\bar{q}_{\max}$ constraint when the maneuver ends. In addition, because the aerodynamic forces attain a maximum value, gravity can be neglected. At last, we assume the pull up ends where the $\dot{q}_{\mathrm{TPS}}$ and $\bar{q}_{\max}$ curves intersect. Although no feasible maneuver exists matching this assumption, it allows one to derive a simple end density estimate. Hence, Eq. (11) can be modified to get

$$\frac{1}{6}\ \ell_n\left(\frac{\rho_2}{\tilde{\rho}}\right) + \frac{3\rho_2 - \tilde{\rho}}{\beta B \cdot L_T/D} = 0 \tag{21}$$

A simple ρ_2 estimate can be achieved noting that a solution to Eq. (21) exists if and only if $1/3 < \rho_2/\tilde{\rho} < 1$. The pull up should start at $\tilde{\rho}/3$ in case of zero $L_T/D \cdot B$, whereas infinite $L_T/D \cdot B$ would allow performing the maneuver instantaneously at $\tilde{\rho}$. To achieve a reasonable compromise between model accuracy and simplicity, the $\rho_2/\tilde{\rho}$ ratio is assumed to be constant and equal to $3/4$ [Eq. (22)]. It is worth noting that this ρ_2 estimate can be either conservative or not, depending on $L_T/D \cdot B$ and $\tilde{\rho}$. However, for a given $\tilde{\rho}$, the estimate becomes more conservative as $L_T/D \cdot B$ increases.

$$\rho_q = 3/4 \cdot (\sqrt{2\bar{q}_{\max}}/k)^3 \tag{22}$$

The maximum density at which the TPS test can be performed is also affected by the vehicle's capability to track the constant-$\dot{q}_{\mathrm{TPS}}$ trajectory, as has been shown in Sec. II.A. More precisely, the TPS test can be carried out only within a limited density range, dictated by

Table 1 Test cases main features

Test cases	L_T/D	R_N, cm	$\dot{q}_{\mathrm{TPS}}$, kW/m^2	$\bar{q}_{\max}$, kPa	E, MJ/kg	h_A, km
No. 1 Mini-SRT	2.4	1.0	500	130.0	3.75	120.0
No. 2 SHARP-L1, Michael trajectory	3.3	0.6	600	50.0	4.37	58.0
No. 3 SHARP-L1, Malmstrom trajectory	3.3	0.6	1000	43.0	9.60	71.5

the vehicle's ballistic coefficient and aerodynamic efficiency. The minimum trackable density is not of concern, because it will surely be smaller than the thermal trim acquisition one. On the contrary, the maximum trackable density can be evaluated solving Eq. (9) with a numeric root finding scheme. The maximum density at which the TPS test can be performed ρ_2 is thus given by the minimum between those specified by the $\bar{q}_{\max}$ constraint and the $\dot{q}_{\mathrm{TPS}}$ tracking requirement:

$$\rho_2 = \min\{\rho_q, \rho_T\} \tag{23}$$

To obtain the optimal trajectory, the variables to be optimized are the trajectory inputs L/D and B. However, given the approximate point mass dynamics model introduced in the previous sections, the inputs are determined once the pull-up maneuver vertical lift-to-drag ratio is specified. Indeed, the ballistic coefficient is determined by L/D_{PU} from Eqs. (13) and (14), and L/D_{TPS} is univocally determined by the ballistic coefficient via the heat flux tracking condition [Eq. (8)]. As a consequence, the optimization problem can be formulated as searching for the pull-up maneuver vertical lift-to-drag ratio that maximizes the TPS testing time Δt, under the dynamics constraint Eqs. (13–16) and (18), path constraints, whose effect has been modeled with Eq. (23), and for a given initial state at the apogee:

$$\Delta t\left(L/D_{\mathrm{PU}}^{\mathrm{Opt}}\right) = \max_{L/D_{\mathrm{PU}} \in [-L_T/D, L_T/D]} \Delta t(L/D_{\mathrm{PU}}) \tag{24}$$

subject to Eqs. (13–16), (18), and (23), and $x(t_A) = x_A$.

Solving problem (24) is not a trivial task, because, in general, ρ_2 depends nonlinearly on L/D_{PU} via the ballistic coefficient B. Nevertheless, if the $\dot{q}_{\mathrm{TPS}}$ tracking specifies a maximum TPS test density higher than the dynamic pressure constraint, the L/D_{PU} does not affect ρ_2. As will be shown in the last section of this paper, this condition occurs for the majority of the cases having practical interest, allowing the ρ_2 dependency on L/D_{PU} to be neglected. With this assumption, it can be easily demonstrated that the merit function is a monotone increasing function of L/D_{PU}, whose optimal value is thus the maximum allowable $L/D_{\mathrm{PU}}^{\mathrm{Opt}} = L_T/D$.

In synthesis, given a vehicle's aerodynamic shape, the optimal trajectory is obtained flying at the maximum vertical lift-to-drag ratio, and at zero bank up to the heat flux trim acquisition point. Heat flux trim is guaranteed by the appropriate selection of the surface-to-mass ratio, that is, such to comply with Eqs. (13) and (14). Then, the bank angle has to be instantaneously changed and eventually modulated to exert the L/D_{TPS} required to track the constant-$\dot{q}$ trajectory segment, up to the maximum allowed density ρ_2.

IV. Approximate Model Validation

The proposed model's applicability and effectiveness is verified by comparison with the trajectories obtained employing a standard numerical optimization technique. With the present method being a mission design tool, we expect that the approximate model preserves the main features of the optimal trajectories, but introduces some acceptable degree of approximation with respect to numeric solutions.

The numeric trajectories we consider for the comparative analysis are derived by solving a local optimization problem using a standard direct collocation scheme [23]. The vehicle's motion is obtained as the numeric solution of a conventional point mass 3-DOF translational model of an atmospheric entry on a spherical planet, under angle of attack and bank angle guidance [24]. For comparison purposes, results are shown only in terms of longitudinal variables. The US76 standard atmosphere model is employed to compute relevant variables, and table data are used to determine the aerodynamic forces as a function of Mach number and angle of attack.

The numeric optimization problem searches for the constant angle of attack value, the vehicle's mass, and the piecewise linear bank angle time profile that maximize the time interval in which the thermal flux is equal to the TPS test one within a given tolerance. Path constraints are enforced in terms of the maximum stagnation point heat flux, limited to be lower than $\dot{q}_{\mathrm{TPS}}$, the maximum dynamic pressure, and a maximum bank angle rate, to model the effects of noninstantaneous rotational dynamics [25]. The initial state is taken at the trajectory apogee, and the final state occurs when the flight path becomes horizontal. The latter choice allows one to include in the numeric solution also the dynamic pressure constraint compliance maneuver. Indeed, limitation of the maximum dynamic pressure causes a pull-up maneuver after the constant heat flux phase, which results in a subsequent γ increase up to positive values.

The comparison is carried out considering three test cases, selected to be representative of the missions the method has been designed for, namely low-energy suborbital TPS flight tests. Their main characteristics are collected in Table 1 and are thought to cover a wide range of possible applications, at least in terms of maximum thermal flux, dynamic pressure, and initial state at the apogee. Case no. 1 is derived from the mini-SRT project [10], a feasibility study for a small-scale winged vehicle performed by the authors under funding by CIRA. Cases 2 and 3 refer to the same vehicle, SHARP-L1 [11,26], a wave rider configuration originally conceived as a follow-on of the SHARP B1 and B2 ballistic vehicles. These two cases differ in the initial states, which are taken from the X-33 suborbital trajectories studies available in open literature [16]. The two points of the X-33 trajectories have been used only because of their suborbital mechanical energy content, despite the fact that the trajectories we obtained in this paper bear no similarity with the X-33 ones that were designed to meet completely different requirements subject to dissimilar constraints. In particular, X-33 entry trajectories to the Michael Army Air Field and Malmstrom Air Force Base have been used for the intial states of cases 2 and 3, respectively.

Results demonstrate the approximate method preserves the key features of the trajectories obtained by the standard numeric solution technique. Indeed, the analytic L/D, V, and γ profiles versus ρ, shown in Figs. 2–4, match the numeric ones within an accuracy typical of a mission design phase. In particular, it can be seen that the pull-up vertical lift-to-drag ratio derived with the approximate method is in excellent agreement with the numeric one. As expected, in the numeric trajectory the vertical lift is reduced before the analytic one, because of the effect of noninstantaneous rotational dynamics. In the successive TPS test phase the analytic solution envelops the numeric one, even though discrepancies can be observed in the TPS test end density. We remark that the approximate trajectory is shown up to this density value, computed via Eq. (23). The numeric solution instead includes also the dynamic pressure constraint compliance maneuver, represented in Fig. 2 by a sudden increase in L/D.

A comparison of the resulting trajectory inputs, TPS test end density, and test time is given in Table 2. The analytic solution percentage variation with respect to the numeric ones is also shown. It is worth noting that the B and L/D_{PU} values obtained by numerical simulations vary with density. Thus, for comparison purposes, the mean values of these two inputs on the relevant density domain are used in Table 2. Results confirm that in all the considered test cases the optimal pull-up maneuver requires maximum use of the aerodynamic efficiency in the positive vertical direction (i.e., zero bank flight), as predicted by the approximate method. The accuracy

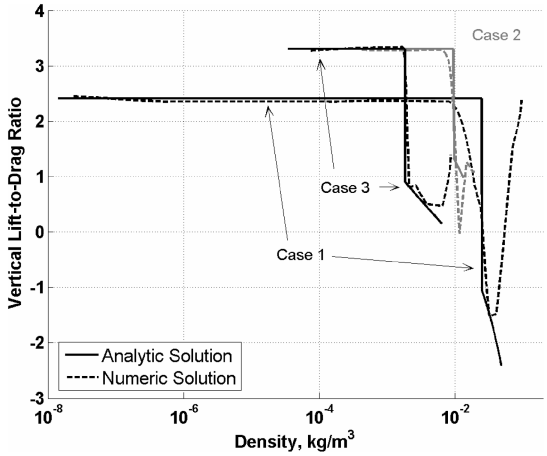

Fig. 2 Analytic vs numeric vertical lift-to-drag ratio–density profiles.

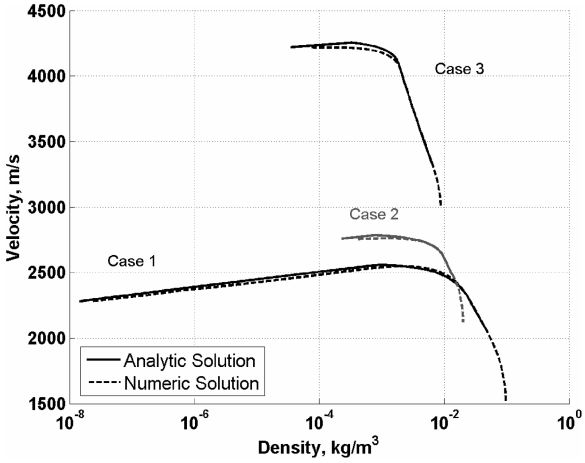

Fig. 3 Analytic vs numeric velocity–density profiles.

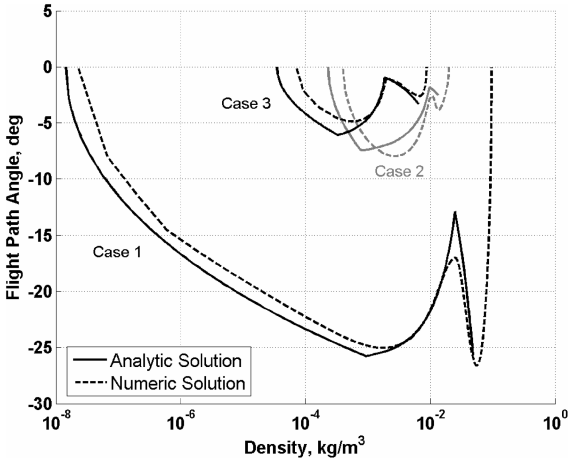

Fig. 4 Analytic vs numeric flight path angle–density profiles.

in the ballistic coefficient exhibits a certain degree of variability. Specifically, the differences between cases 1 and 3 arise from the different γ profiles, which affect the magnitude of the error introduced by neglecting the gravity tangential component. Case 2 shows a ballistic coefficient substantially higher than the other cases. In these conditions, the analytic method considerably overestimates the ballistic coefficient, because the Keplerian to atmospheric flight patching condition is expressed in terms of dynamic pressure. Indeed, the higher B is, the smaller the drag deceleration sensed by the vehicle at a certain dynamic pressure. The resulting effect is to neglect the positive tangential gravity earlier than the other two cases, yielding a further increase in the analytically computed B. Concerning the TPS test time, modeling errors tend to balance each other yielding a more accurate Δt estimation. For instance, overestimating B may cause either an increase or a decrease in Δt, due to the dependency on B in Eq. (7) and its effect on the ρ_q estimate, respectively.

The previous analysis suggests that the semi-analytic method can adequately describe suborbital TPS flight tests trajectories for mission design purposes. Notwithstanding all the introduced approximations and the inability of analytical models to cope with angular rate limitations, the method captures the essential features of the optimal trajectories. When compared to the numeric approaches, the method proves to estimate the TPS test time and the required pull-up vertical lift-to-drag ratio with good accuracy. The accuracy in estimating the ballistic coefficient is instead variable with B itself, and it degrades as B increases.

V. Mission Design Space Analysis

The ultimate goal of the proposed model is to perform parametric analyses in a preliminary design phase, to draw meaningful indications on promising mission and system design candidates. This is done by determining the apogee conditions required to carry out a certain TPS test, given the reentry vehicle characteristics. The knowledge of the apogee conditions helps in selecting the ascent vehicle that has a considerable effect on mission cost and complexity, and thus on weighing different design options.

In the approximate model, the TPS test and vehicle features are defined in terms of the desired heat flux and test time, the maximum admissible dynamic pressure, the vehicle's aerodynamic efficiency, and the stagnation point radius. Once these parameters have been set, the apogee conditions that realize the desired mission can be obtained if the ballistic coefficient is specified. Because the ballistic coefficient is a design variable, the described approach can be used to perform parametric analyses varying B in a predetermined range.

The process yielding to the apogee conditions from the knowledge of the ballistic coefficient is described by the flowchart in Fig. 5. Once a certain B is fixed, the apogee energy and altitude needed to perform the desired mission are determined by inversion of the model equations listed in Fig. 5. Most of the equations can be inverted analytically. The maximum density at which the vehicle can track the heat flux trim conditions has to be determined solving Eq. (9) by means of a numeric root finding scheme. The Keplerian to atmospheric motion interface density needs to be determined by numeric means as well.

To demonstrate the method effectiveness, a parametric analysis is carried out, using realistic values of the parameters characterizing suborbital TPS test missions as follows: $R_N = 1.0$ cm, $\dot{q}_{\mathrm{TPS}} = \{600, 1000\}$ kW/m^2, $\bar{q}_{\max} = [50, 100]$ kPa, $L_T/D = \{1, 3\}$,

Table 2 Analytic vs numeric solution: main features comparison

	Case 1			Case 2			Case 3		
	Analytic	Numeric	% Variation	Analytic	Numeric	% Variation	Analytic	Numeric	% Variation
Δt, s	6.34	6.29	0.8	21.83	24.22	−9.9	75.32	83.38	−9.7
L/D_{PU}	2.41	2.36	2.1	3.30	3.28	0.6	3.30	3.33	−0.9
B, kg/m^2	2146.8	1704.1	26.0	5888.8	3980.3	47.9	2208.5	2435.2	−9.3
ρ_2, kg/m^3	4.84e − 2	5.01e − 2	−3.4	1.34e − 2	1.56e − 2	−14.1	6.39e − 3	6.54e − 3	−2.3

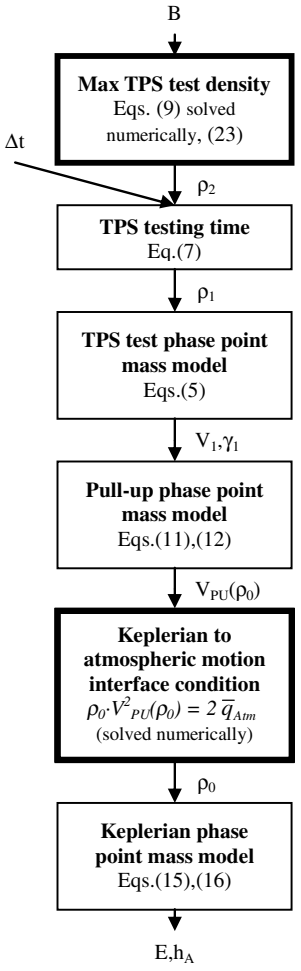

Fig. 5 Mission design flowchart.

$\Delta t = [30, 100]$ s, $B = [10^3, 10^4]$ kg/m^2. In all of the analyses the stagnation point radius is taken equal to 1 cm. Indeed, to take advantage from the higher resulting heat fluxes, sharp edges seem to be an obliged choice for suborbital TPS flight tests. Although small samples may be satisfactory for materials testing, system-level testing may require flight size TPS components, for example, to enable investigations of interface issues, and thus higher R_N values. Although not shown here for brevity, apogee conditions required by these applications can be determined taking advantage of the present method. For the parametric analysis, two different test heat flux values are investigated, representative of the typical aerothermal environment in lifting reentry [9] and compatible with advanced TPS material capabilities [27]. In addition, we will consider vehicles capable of flying at high dynamic pressures, in order to limit the apogee specific mechanical energies to suborbital values. We thus consider maximum dynamic pressure constraints ranging from 50 to 100 kPa. Two different aerodynamic efficiencies are analyzed, $L_T/D = 1$ and 3, related to different aerodynamic shapes. The latter is representative of winged or lifting body configurations, whereas the former might be the efficiency of a biconic shape at nonzero angle of attack. In order for the TPS test to be of interest, a minimum test duration of 30 s is assumed. On the other hand, we limit the test duration to 100 s, because for longer times the integrated heat load could be of concern for the vehicle design. For instance, if the vehicle flies the 1 MW/m^2 heat flux for the maximum test duration the integrated heat load would reach 100 MJ/m^2 only in the TPS test phase, which is a nonnegligible fraction of typical lifting reentry heat loads [9,11]. Finally, the parametric analysis is conducted for ballistic coefficients ranging within 10^3–10^4 kg/m^2, representative of physically realizable vehicles for this kind of application.

Figure 6 shows the typical effect of Δt and B on apogee conditions, where the velocity is used in place of the specific mechanical energy. Indeed, expressing the results in terms of the apogee velocity allows a simpler intuitive interpretation. In addition, in suborbital flights the main contribution to the specific mechanical energy is the kinetic one; thus velocity is in practice proportional to $\sqrt{E}$. The parametric diagram shows that higher test times require higher velocities and smaller apogee altitudes. This effect becomes less significant as the ballistic coefficient increases. Results show that vehicles with high B values are preferable, being able to perform the TPS test starting from smaller specific mechanical energies.

The effect of the maximum dynamic pressure constraint is shown in Fig. 7, for a single $\dot{q}_{\mathrm{TPS}}$, L_T/D, and Δt combination. Increasing the maximum sustainable dynamic pressure allows reducing the specific kinetic energy at the apogee, whereas the apogee altitude has to be raised. This results into a lower specific mechanical energy, especially for high B values that are preferable for energy minimization.

Figure 8 shows the maximum trackable densities as given by the $\dot{q}_{\mathrm{TPS}}$ tracking requirement [Eq. (9)] and the dynamic pressure constraint compliance maneuver [Eq. (22)]. It is worth noting that, as anticipated in Sec. III, the maximum TPS test density is dictated by the dynamic pressure constraint in almost all the analyzed cases. Indeed, even considering the biggest ρ_q, arising from the highest $\bar{q}_{\max}$, the density value given by the $\dot{q}_{\mathrm{TPS}}$ tracking requirement is almost always higher than ρ_q. There are only a limited number of conditions in which this is not true, occurring for low B–low L_T/D values, thus having a limited practical interest.

Different mission design options can be compared using apogee velocity and altitude parametric diagrams. As an example, Figs. 9 and 10 collect the diagrams of different design options for a 600 kW/m^2 test heat flux. The low aerodynamic efficiency, low

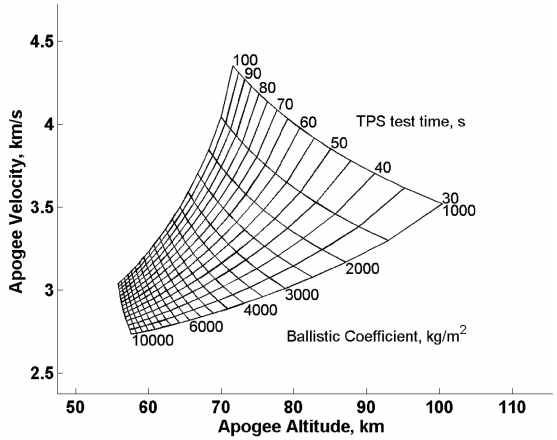

Fig. 6 Δt and B parametric effect on apogee conditions; $\dot{q}_{\mathrm{TPS}} = 600$ kW/m^2, $L_T/D = 3$, and $\bar{q}_{\max} = 100$ kPa.

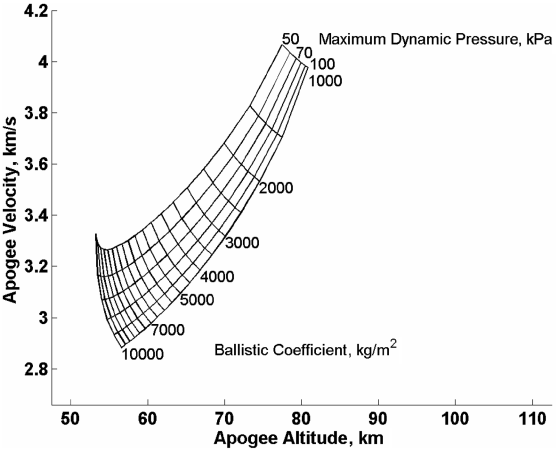

Fig. 7 Dynamic pressure constraint effect on apogee conditions; $\dot{q}_{\mathrm{TPS}} = 600$ kW/m^2, $L_T/D = 3$, and $\Delta t = 60$ s.

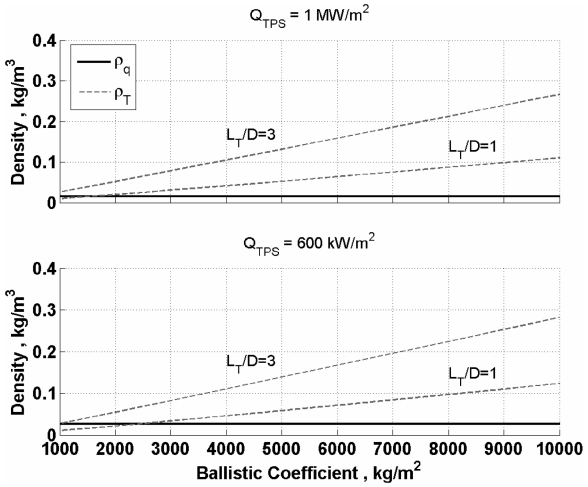

Fig. 8 Dynamic pressure constraint compliance vs maximum trackable densities; $\bar{q}_{\max} = 100$ kPa.

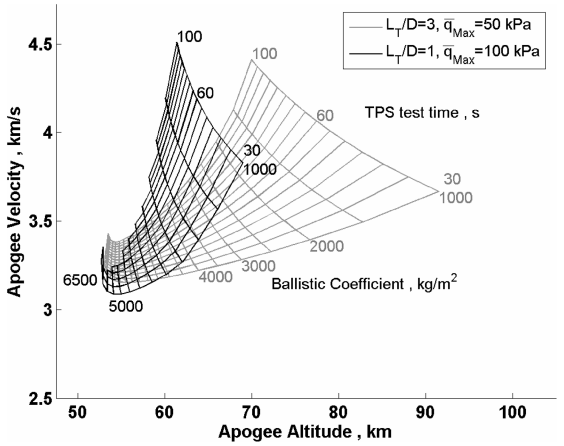

Fig. 9 Apogee conditions for different design options; $\dot{q}_{\mathrm{TPS}} = 600$ kW/m^2.

maximum dynamic pressure case is not shown, given the unfavorable effect of this combination on the apogee conditions. In addition, low aerodynamic efficiency vehicles can be designed to withstand a high dynamic pressure flight more easily than winged ones. Results show that low L_T/D vehicles are not capable of reaching the required heat flux trim conditions if their ballistic coefficient is higher than $\sim$6000 kg/m^2. Even for lower B values the maximum achievable test duration can be shorter than 100 s.

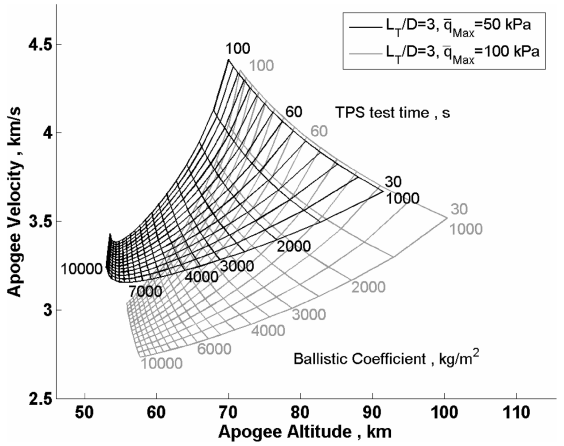

Fig. 10 Apogee conditions for different design options; $\dot{q}_{\mathrm{TPS}} = 600$ kW/m^2.

Table 3 Example apogee conditions; $\dot{q}_{\mathrm{TPS}} = 600$ kW/m^2, $B = 5000$ kg/m^2, and $\Delta t = 30$ s.

L_T/D	$\bar{q}_{\max}$, kPa	V_A, m/s	h_A, km	E, MJ/kg
1	100	3089.7	55.0	5.31
3	100	2860.1	68.9	4.76
3	50	3186.8	60.5	5.67

Interestingly, in this design option there is a B value that minimizes the Keplerian phase specific mechanical energy, equal to $\sim$5000 kg/m^2 for test times around 30 s. The existence of an optimal ballistic coefficient is justified by the complex dependency of initial conditions on B that causes opposite effects. For instance, increasing B allows one to start the TPS test at a lower velocity, with a consequent reduction in the required initial energy. Conversely, a higher energy is needed to perform a given pull up with a vehicle less sensible to aerodynamic accelerations.

The comparison with the other two design options shows that the advantage of operating with a higher maneuverability vehicle (L_T/D 1 versus 3) is lost if the maximum sustainable dynamic pressure is halved. Indeed, if B is higher than $\sim$2500 kg/m^2, the low L_T/D, high $\bar{q}_{\max}$ option yields lower apogee energies. Nevertheless, if the higher aerodynamic efficiency vehicle can withstand the same dynamic pressure, this option is the most favorable because the same TPS test can be performed with a smaller apogee energy. For completeness, the three design options are compared in Table 3, showing the apogee conditions required when $B = 5000$ kg/m^2 and $\Delta t = 30$ s.

From the previous analysis the maximum dynamic pressure turns out to have a significant effect on the achievable performance. For this reason, results of the more demanding 1 MW/m^2 case study, shown in Fig. 11, are plotted only for vehicles capable of withstanding a dynamic pressure of 100 kPa. The low maneuverability alternative is unable to pull up to the desired heat flux trim conditions for ballistic coefficients higher than $\sim$2500 kg/m^2. Moreover, the high L_T/D vehicle exhibits an optimal B value around 6000–6500 kg/m^2 that slightly depends on the desired test duration. Because this vehicle option also has the highest performances among the analyzed ones, we can conclude that for TPS testing at $\dot{q}_{\mathrm{TPS}} = 1$ MW/m^2, there are optimal vehicle designs in the investigated parameters ranges that minimize the specific mechanical energy at the trajectory apogee. Their main features are collected in Table 4 for minimum and maximum TPS test durations.

VI. Conclusions

An approximate methodology has been developed and validated that identifies an optimal mission profile for an advanced TPS suborbital flight test, designed to expose a specific area of the vehicle

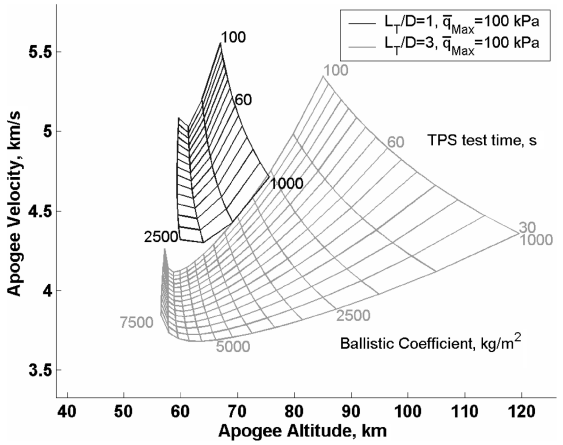

Fig. 11 Apogee conditions for different design options; $\dot{q}_{\mathrm{TPS}} = 1000$ kW/m^2.

Table 4 Optimal mission designs; $\dot{q}_{TPS} = 1$ MW/m^2, $\bar{q}_{max} = 100$ kPa, $L_T/D = 3$.

Δt, s	B, kg/m^2	V_A, m/s	h_A, km	E, MJ/kg
30	5934	3681.3	61.7	7.38
100	6467	4116.5	58.8	9.04

to a constant heat flux. The methodology requires the numeric solution of two scalar nonlinear equations and the a priori knowledge only of high level mission requirements, such as the desired TPS test heat flux. These features make it appealing to perform parametric analyses in broad regions of the mission design space, to limit promising design candidates to an extent manageable by conventional numeric-simulation-based methods. The approximate method is capable of identifying with a minimum effort the trajectory apogee conditions required to perform the test as desired. This information is of great usefulness in selecting the needed launch vehicle. Indeed, the apogee conditions achievable by a generic rocket can be evaluated in a relatively straightforward manner, and then compared to those computed by the approximate method.

To demonstrate its effectiveness, a mission analysis has been performed using reasonable ranges of relevant parameters. Results show that needed apogee conditions considerably differ from the ones provided by existing off-the-shelf vectors. For instance, sounding rockets, that seem the most convenient choice for cost constriction, could attain the needed specific mechanical energies, but are designed for considerably higher apogee altitudes. Their possible adaptation to the required apogee conditions would call for major changes, even at a system level. Therefore, even if the ascent vehicle selection is beyond the scope of this work, the use of the proposed method suggests that a consistent effort would be required to obtain the constant heat flux TPS test apogee conditions with off-the-shelf rockets. Nevertheless, the constant heat flux flight test can be weighed against other TPS testing alternatives taking advantage of the proposed tool.

In terms of the entry phase mission design, results point out that increasing the vehicle's ballistic coefficient allows reducing the specific mechanical energy at reentry, even though there is a superior limit above which this behavior is reversed. The maximum admissible dynamic pressure turns out to have a primary effect on the TPS testing capabilities of a candidate design. For instance, cases are shown in which a biconic shaped vehicle can accomplish the same mission of a winged one with smaller launch energies, because it is capable of withstanding a higher dynamic pressure.

Finally, the proposed tool is capable of identifying the existence of optimum solutions in the mission design space. Indeed, concerning test heat fluxes around 1 MW/m^2, representative of limit capabilities of novel TPS ceramic materials, an optimal mission design is found in the investigated parameter region. Specifically, results show that using the optimal design to reproduce this severe aerothermal environment for 100 s requires an apogee specific mechanical energy 30% lower than the circular orbit one at the same altitude.

References

[1] Vennemann, D., "Hypersonic Test Facilities Available in Western Europe for Aerodynamic/Aerothermal and Structure/Material Investigations," *Philosophical Transactions: Mathematical, Physical and Engineering Sciences*, Vol. 357, No. 1759, Aug. 1999, pp. 2227–2248.

[2] Stewart, D., "Thermal Protection System Evaluation Using Arc-Jet Flows: Flight Simulation or Research Tool?," *Proceedings of the 105th Annual Meeting and Exposition of the American Ceramic Society*, American Ceramic Society, Westerville, OH, 2003.

[3] Yoshinaga, T., Tate, A., Watanabe, M., and Shimoda, T., "Orbital Re-Entry Experiment Vehicle Ground and Flight Dynamic Test Results Comparison," *Journal of Spacecraft and Rockets*, Vol. 33, No. 5, 1996, pp. 635–642.

[4] Muylaert, J., Cipollini, F., Tumino, G., Kordulla, W., Saccoccia, G., Stavrinidis, C., Caporicci, M., Walpot, L., and Ottens, H., "Preparing for Atmospheric Reentry with EXPERT's Help—An Aerothermodynamic In-Flight Research Programme," *ESA Bulletin*, Vol. 114, May 2003, pp. 42–48, http://www.esa.int/esapub/bulletin/bullet114/chapter4_bul114.pdf.

[5] Anon., "SOAREX (Sub-Orbital Aerodynamic Re-Entry EXperiments)," NASA Ames Technology Capabilities and Facilities [online database], http://www.nasa.gov/centers/ames/research/technology-onepagers/soarex.html [retrieved 1 Aug. 2007].

[6] Eggers, T., Longo, J., Hoerschgen, M., and Stamminger, A., "The Hypersonic Flight Experiment SHEFEX," *AIAA/CIRA 13th International Space Planes and Hypersonics Systems and Technologies Conference*, AIAA, Reston, VA, 16–20 May 2005.

[7] Rasky, D., Salute, J., Kolodziej, P., and Bull, J., "The NASA Sharp Flight Experiment," *3rd European Workshop on Thermal Protection Systems*, ESA, Noordwijk, The Netherlands, 25–27 March 1998.

[8] Russo, G., "USV Flying Test Beds for Future Generations LV Technology Development," AIAA Paper 2003-6978, Dec. 2003.

[9] Ried, R. C., "Orbiter Entry Aerothermodynamics," *Space Shuttle Technical Conference*, CP-2342, NASA, Pt. 2, 1983, pp. 1051–1061.

[10] Tancredi, U., Accardo, D., Grassi, M., and Curreri, F., "Unmanned Space Vehicle Technology Demonstrator," *Acta Astronautica*, Vol. 60, No. 3, 2007, pp. 186–197.

[11] Tillier, C. E., "Simulation-Based Analysis of Reentry Dynamics for the Sharp Atmospheric Entry Vehicle," NASA CR-1998-208334, 1998.

[12] Betts, J. T., "Survey of Numerical Methods for Trajectory Optimization," *Journal of Guidance, Control, and Dynamics*, Vol. 21, No. 2, 1998, pp. 193–207.

[13] Murray, J. E., and Tartabini, P. V., "Development of a Mars Airplane Entry, Descent, and Flight Trajectory," NASA TM-2001-209035, 2001.

[14] Griffin, M. D., and French, J. R., *Space Vehicle Design*, AIAA Education Series, AIAA, Washington, D.C., 1991, Chaps. 5, 6.

[15] Harpold, J. D., and Graves, C. A., Jr., "Shuttle Entry Guidance," *Journal of the Astronautical Sciences*, Vol. 27, No. 3, 1979, pp. 239–268.

[16] Lu, P., and Hanson, J. M., "Entry Guidance for the X-33 Vehicle," *Journal of Spacecraft and Rockets*, Vol. 35, No. 3, 1998, pp. 342–349.

[17] Zimmerman, C., Dukeman, G., and Hanson, J., "Automated Method to Compute Orbital Reentry Trajectories with Heating Constraints," *Journal of Guidance, Control, and Dynamics*, Vol. 26, No. 4, 2003, pp. 523–529.

[18] Savino, R., De Stefano Fumo, M., Paterna, D., and Serpico, M., "Aerothermodynamic Study of UHTC-Based Thermal Protection Systems," *Aerospace Science and Technology*, Vol. 9, No. 2, 2005, pp. 151–160.

[19] Kuntz, D., and Potter, D., "Boundary Layer Transition and Hypersonic Flight Testing," AIAA Paper 2007-308, Jan. 2007.

[20] Fay, J. A., and Riddell, F. R., "Theory of Stagnation Point Heat Transfer in Dissociated Air," *Journal of Aeronautical Sciences*, Vol. 25, Feb. 1958, pp. 73–85.

[21] Loh, W. H. T., *Re-Entry and Planetary Entry Physics and Technology*, Springer–Verlag, New York, 1968.

[22] Regan, F. J., and Anandakrishnan, S. M., *Dynamics of Atmospheric Re-Entry*, AIAA Education Series, AIAA, Washington, D.C., 1993, Chaps. 6, 7.

[23] Hull, D. G., "Conversion of Optimal Control Problems into Parameter Optimization Problems," *Journal of Guidance, Control, and Dynamics*, Vol. 20, No. 1, 1997, pp. 57–60.

[24] Vinh, N. X., Busemann, A., and Culp, R. D., *Hypersonic and Planetary Entry Flight Mechanics*, Univ. of Michigan Press, Ann Arbor, MI, 1980, pp. 26–27.

[25] Jits, R. Y., and Walberg, G. D., "Blended Control, Predictor-Corrector Guidance Algorithm: An Enabling Technology for Mars Aerocapture," *Acta Astronautica*, Vol. 54, No. 6, 2004, pp. 385–398.

[26] Kolodziej, P., Bowles, J. V., Brown, J. L., Cornelison, C. J., Lawrence, S. L., Loomis, M. P., Merriam, M. L., Rasky, D. J., Tam, T. C., and Wercinski, P. F., "Sharp-L1 Technology Demonstrator Development —An Aerothermodynamic Perspective," AIAA Paper 2000-2688, 2000.

[27] Ogasawara, K., Nagase, T., Yamao, H., and Fujii, K., "Reentry Vehicle Crossrange Ability Improvement by Using High Temperature Ceramics," *11th AIAA/AAAF International Conference, Space planes and Hypersonic Systems and Technologies*, AIAA, Reston, VA, Oct. 2002.

K. Wurster
Associate Editor